References and Notes

1. N. Ban, P. Nissen, J. Hansen, P. B. Moore, T. A. Steitz, *Science* **289**, 905 (2000).
2. B. T. Wimberly *et al.*, *Nature* **407**, 327 (2000).
3. M. M. Yusupov *et al.*, *Science* **292**, 883 (2001); published online 29 March 2001 (10.1126/science.1060089).
4. B. S. Schuwirth *et al.*, *Science* **310**, 827 (2005).
5. K. Mitra, J. Frank, *Annu. Rev. Biophys. Biomol. Struct.* **35**, 299 (2006).
6. A. Nikulin *et al.*, *Nat. Struct. Biol.* **10**, 104 (2003).
7. M. Diaconu *et al.*, *Cell* **121**, 991 (2005).
8. Materials and methods are available as supporting material on *Science* Online.
9. L. Jenner *et al.*, *Science* **308**, 120 (2005).
10. J. Harms *et al.*, *Cell* **107**, 679 (2001).
11. J. M. Ogle, F. V. Murphy, M. J. Tarry, V. Ramakrishnan, *Cell* **111**, 721 (2002).
12. D. Moazed, H. F. Noller, *Nature* **342**, 142 (1989).
13. J. M. Ogle *et al.*, *Science* **292**, 897 (2001).
14. U. L. RajBhandary, C. M. Chow, in *tRNA: Structure, Biosynthesis and Function*, D. Söll, U. L. RajBhandary, Eds. (American Society for Microbiology Press, Washington, DC, 1995), pp. 511–528.
15. E. Schmitt, M. Panvert, S. Blanquet, Y. Mechulam, *EMBO J.* **17**, 6819 (1998).
16. U. von Ahsen, H. F. Noller, *Science* **267**, 234 (1995).
17. N. M. Abdi, K. Fredrick, *RNA* **11**, 1624 (2005).
18. P. Nissen, J. A. Ippolito, N. Ban, P. B. Moore, T. A. Steitz, *Proc. Natl. Acad. Sci. U.S.A.* **98**, 4899 (2001).
19. D. J. Battle, J. A. Doudna, *Proc. Natl. Acad. Sci. U.S.A.* **99**, 11676 (2002).
20. L. Lancaster, H. F. Noller, *Mol. Cell* **20**, 623 (2005).
21. J. Frank, R. K. Agrawal, *Nature* **406**, 318 (2000).
22. A. P. Carter *et al.*, *Nature* **407**, 340 (2000).
23. L. Jovine, S. Djordjevic, D. Rhodes, *J. Mol. Biol.* **301**, 401 (2000).
24. H. Shi, P. B. Moore, *RNA* **6**, 1091 (2000).
25. T. M. Schmeing *et al.*, *Nat. Struct. Biol.* **9**, 225 (2002).
26. T. M. Schmeing, K. S. Huang, S. A. Strobel, T. A. Steitz, *Nature* **438**, 520 (2005).
27. A. Bashan *et al.*, *Mol. Cell* **11**, 91 (2003).
28. J. S. Weinger, K. M. Parnell, S. Dorner, R. Green, S. A. Strobel, *Nat. Struct. Mol. Biol.* **11**, 1101 (2004).
29. M. D. Erlacher *et al.*, *Nucleic Acids Res.* **33**, 1618 (2005).
30. S. V. Kirillov, J. Wower, S. S. Hixson, R. A. Zimmermann, *FEBS Lett.* **514**, 60 (2002).
31. B. A. Maguire, A. D. Beniaminov, H. Ramu, A. S. Mankin, R. A. Zimmermann, *Mol. Cell* **20**, 427 (2005).
32. H. Wang *et al.*, *Protein Sci.* **13**, 2806 (2004).
33. U. Geigenmuller, K. H. Nierhaus, *EMBO J.* **9**, 4527 (1990).
34. D. Moazed, H. F. Noller, *Cell* **57**, 585 (1989).
35. Y. P. Semenkov, M. V. Rodnina, W. Wintermeyer, *Proc. Natl. Acad. Sci. U.S.A.* **93**, 12183 (1996).
36. R. Lill, J. M. Robertson, W. Wintermeyer, *EMBO J.* **8**, 3933 (1989).
37. J. S. Feinberg, S. Joseph, *Proc. Natl. Acad. Sci. U.S.A.* **98**, 11120 (2001).
38. T. M. Schmeing, P. B. Moore, T. A. Steitz, *RNA* **9**, 1345 (2003).
39. G. Z. Yusupova, M. M. Yusupov, J. H. Cate, H. F. Noller, *Cell* **106**, 233 (2001).
40. M. Osswald, B. Greuer, R. Brimacombe, *Nucleic Acids Res.* **18**, 6755 (1990).
41. J. W. Kenny, R. R. Traut, *J. Mol. Biol.* **127**, 243 (1979).
42. A. J. Eistetter, P. D. Butler, R. R. Traut, T. G. Fanning, *FEMS Microbiol. Lett.* **180**, 345 (1999).
43. T. Hard, A. Rak, P. Allard, L. Kloo, M. Garber, *J. Mol. Biol.* **296**, 169 (2000).
44. F. C. Chao, *Arch. Biochem. Biophys.* **70**, 426 (1957).
45. J. Frank *et al.*, *Biochem. Cell Biol.* **73**, 757 (1995).
46. S. Ghosh, S. Joseph, *RNA* **11**, 657 (2005).
47. W. L. DeLano, http://pymol.sourceforge.net/ (2006).

48. Crystals were screened at Daresbury Labs, UK, or at European Synchrotron Radiation Facility (ESRF), Grenoble, France. Data were collected at the Swiss Light Source, Paul Scherrer Institut, Villigen, Switzerland, and at ESRF. We thank C. Schulze-Briese and R. Ravelli for help and advice with data collection; W. Kabsch for advice with the data integration program XDS; P. Adams for advice and for modifying the refinement program CNS; D. Gohara for optimally compiling an operating system X version of this modified CNS; P. Emsley for advice with the graphics program COOT; K. Nierhaus and E. Schmitt for gifts of overproducing clones of Phe- and fMet-tRNAs, respectively; and T. M. Schmeing for critical comments. This work was supported by the Medical Research Council (UK), NIH grant GM67624, the Agouron Institute and fellowships from the Wenner-Gren Foundations (M.S.), the American Cancer Society (C.M.D.), European Molecular Biology Organization (F.V.M.), Austrian Academy of Sciences (A.W.), and the Boehringer-Ingelheim Fond (S.P.). Coordinates and structure factors have been deposited with the Protein Data Bank (PDB) with accession codes 2j00 (30S-1), 2j01 (50S-1), 2j02 (30S-2), and 2j03 (50S-2). V.R. holds stock options in and is on the Scientific Advisory Board of Rib-X Pharmaceuticals, a company that develops antibacterial drugs that target the ribosome.

Supporting Online Material

www.sciencemag.org/cgi/content/full/1131127/DC1
Materials and Methods
Figs. S1 to S5
Tables S1 to S4
References

12 June 2006; accepted 9 August 2006
Published online 7 September 2006;
10.1126/science.1131127
Include this information when citing this paper.

REPORTS

Tunable Quasi–Two-Dimensional Electron Gases in Oxide Heterostructures

S. Thiel,[1] G. Hammerl,[1] A. Schmehl,[2] C. W. Schneider,[1] J. Mannhart[1]*

We report on a large electric-field response of quasi–two-dimensional electron gases generated at interfaces in epitaxial heterostructures grown from insulating oxides. These device structures are characterized by doping layers that are spatially separated from high-mobility quasi–two-dimensional electron gases and therefore present an oxide analog to semiconducting high–electron mobility transistors. By applying a gate voltage, the conductivity of the electron gases can be modulated through a quantum phase transition from an insulating to a metallic state.

Complex oxides show a broad spectrum of intrinsic functionalities, such as ferroelectricity, magnetism, superconductivity, and multiferroic behavior [see (*1*)], which can be used and combined in electronic devices that are based on epitaxially grown heterostructures. Physical properties may arise in such multilayers that are not found in either of their constituents. One example, a conducting quasi–two-dimensional electron gas (q2-DEG) is formed at the interface between the two insulating, dielectric perovskites, $LaAlO_3$ and $SrTiO_3$ (*2*, *3*). The electrons at this interface are highly mobile, with values up to 10^4 cm^2 V^{-1} s^{-1} (4.2 K) having been reported (*2*–*5*), and were found to have densities orders of magnitude higher than the densities of two-dimensional electron gases induced at interfaces in heterostructures based on III-V semiconductors. Exploring whether the q2-DEGs can be applied to fabricate high electron mobility transistor (HEMT)–type field effect devices (*6*), we observed that they can be tuned by altering on the unit cell level the thickness of the $LaAlO_3$ sheets. For $LaAlO_3$ layers that are up to 3 unit cells (uc) thick, highly insulating interfaces are obtained. In field-effect transistor configurations that use such interfaces as drain-source (DS) channels, a phase transition to the conducting state is readily achieved by gate fields. Upon change of their carrier densities with applied electric fields, the q2-DEGs react with a pronounced memory effect.

Previous work revealed the existence of metallic electron gases at $LaTiO_3$-$SrTiO_3$ (*7*) and at $LaAlO_3$-$SrTiO_3$ interfaces (*2*, *3*). Because electron energy loss measurements of $LaTiO_3$-$SrTiO_3$ interfaces showed that the electron gas is confined within a ~2-nm-thick layer (*7*), the gas is described to be quasi–two dimensional. Whereas the $LaTiO_3$-$SrTiO_3$ interface is doped by transfer of electrons from the $LaTiO_3$ to the $SrTiO_3$ (*7*, *8*), for the $LaAlO_3$-$SrTiO_3$ interface two different mechanisms have been reported to generate the gas: In some heterostructures, it was found (*2*, *3*) that the carriers are induced by the polarity discontinuity of the TiO_2-LaO^+ stacking

[1]Experimental Physics VI, Center for Electronic Correlations and Magnetism, Institute of Physics, University of Augsburg, D-86135 Augsburg, Germany. [2]Department of Materials Science and Engineering, Pennsylvania State University, University Park, PA 16802–5005, USA.

*To whom correspondence should be addressed. E-mail: jochen.mannhart@physik.uni-augsburg.de

sequence at the interface, whereas in other samples, in particular those grown under low oxygen pressure, growth-induced oxygen vacancies in the $SrTiO_3$ were the dominant source of doping (*4*, *5*). We chose a third approach to dope the interface. By using the electric-field effect (*9*, *10*), we reversibly induced the q2-DEG in $LaAlO_3$-$SrTiO_3$ interfaces, providing the possibility to tune the carrier density of the q2-DEG without perturbing the microstructure of the interface.

For field-effect doping, it is desirable to use interfaces that have a low carrier density and, in the extreme case, are even insulating. For $LaAlO_3$-$SrTiO_3$ interfaces, this implies limiting possible doping by the polarity discontinuity as well as by oxygen defects. Although doping by oxygen vacancies is reduced if the $SrTiO_3$ is well oxidized, it is preferable to use ultrathin $LaAlO_3$ layers to avoid possible doping by the polarity discontinuity, which would dope the interface if the flow of electrons from the $LaAlO_3$ into the interface is energetically favorable and kinetically possible. In the polarity discontinuity model, the driving mechanism is given by the polar catastrophe (*11*), which leads to an electric potential, V, across the $LaAlO_3$ that diverges with its thickness, d. The heterostructure can avoid the divergence of V by introducing interface roughness, by moving electrons into the interface, and by adding oxygen vacancies (*11*). Because the energy needed to activate $LaAlO_3$ electrons such that they can move does not depend on d, this naïve consideration suggests that d may have to reach a critical value, d_c, for the interface to become doped and hence conducting.

To analyze the properties of the electron gas, we fabricated and measured field effect samples (Fig. 1) with the techniques described in (*12*). To gain information on the strength of doping by oxygen defects in our samples, we analyzed one d = 6 uc sample by cathodoluminescence. Luminescence was observed with minute intensity only: Under standard measurement conditions (*4*), no indications of oxygen defects were observed.

As the measurements show (Fig. 2A), for the interfaces to be conducting, d has to reach a critical thickness, d_c = 4 uc. All samples with $d \geq$ 4 uc were conducting [sheet conductance (σ_s) $\approx 4 \times 10^{-3}$ ohm^{-1} (at 4.2 K) and $\sigma_s \approx 2 \times 10^{-5}$ ohm^{-1} (at 300 K)]; all samples with $d < d_c$, insulating ($\sigma_s < 2 \times 10^{-10}$ ohm^{-1} at all temperatures T). The observation of a d_c of 4 uc is consistent with the observation that the conductivity of $SrTiO_3$-$LaAlO_3$-$SrTiO_3$ heterostructures is reduced if their p and n interfaces are spaced by less than 6 uc (*13*).

Control measurements were performed on samples that were patterned to have conducting interfaces with 5-uc $LaAlO_3$ layers in the areas in which the contacts were placed and subcritical, 2-uc- or 3-uc-thick bridges connecting these areas. These samples are insulating and thereby provide evidence that the critical-thickness phenomenon is not simply caused by an effect that is generated by the contact between the Au and the q2-DEG. Further reference studies on samples contacted without Ar ion–etched holes proved that the conducting layer is not located at the surface of the $LaAlO_3$. The conductivity also does not occur in bulk $SrTiO_3$, as was reported (*14*) for samples grown under less oxidizing conditions. To test for bulk conduction, we removed the surface layer of a conducting sample by polishing. The remaining substrate was highly insulating.

According to Hall measurements done on the conducting samples, their carriers are negatively charged with mobilities of ~1200 cm^2 V^{-1} s^{-1} and ~6 cm^2 V^{-1} s^{-1} at 4.2 K and 300 K, respectively, and densities $n \approx 10^{13}$ cm^{-2} at all T (Fig. 2B). These mobilities are high but lower than the best values reported in literature (*2*–*5*), probably because of the growth conditions used, which were selected to obtain interfaces with low carrier density.

Which information does the steplike dependence of the interface conductance on d provide for the doping mechanisms present in these samples? The d dependence of the interface conductance can only be accounted for by doping from growth-induced oxygen defects, if during sample fabrication oxygen can diffuse well through 3-uc-thick layers but not through 4-uc-thick ones. For this case, one has to expect that $d \geq$ 4 uc samples can be turned into insulators, too, if the diffusion of oxygen through their $LaAlO_3$ layers is enhanced. To test this prediction, we annealed a d = 4 uc sample for 7 days at 400°C in 20 bar of O_2. This oxidation step did not result in an insulating interface but reduced the conductance by a factor of 5 (at all T). It therefore has to be concluded that the d dependence of the interface conductance agrees with the behavior predicted for doping by the polarity discontinuity, although additional doping by oxygen vacancies might still be present.

The insulating samples are well suited to generate and control a q2-DEG by the electric field effect. Electric fields were induced across the $SrTiO_3$ or across the $LaAlO_3$ by applying gate voltages, $V_{G,b}$, to backside contacts of the $SrTiO_3$ or voltages, $V_{G,f}$, to small test contacts silver-

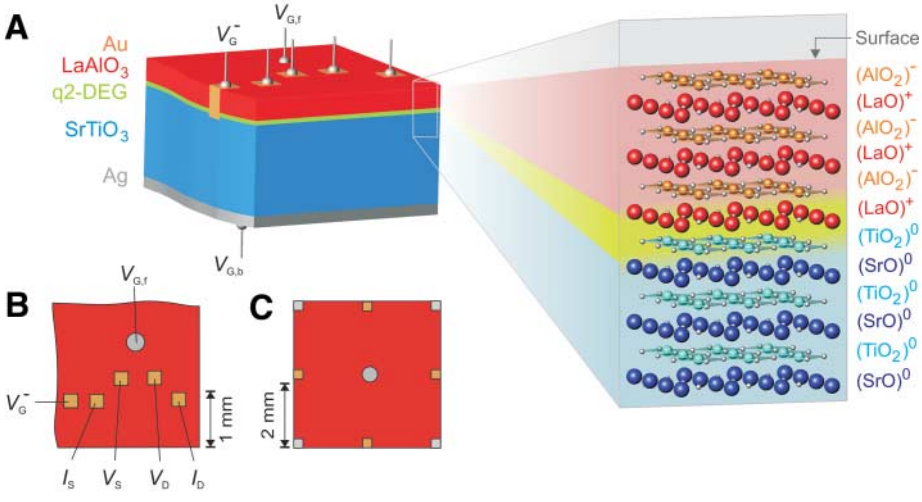

Fig. 1. Sketch of the samples and the contact configurations [the left side of the sample sketch in (**A**) is a cross-sectional cut]. The $SrTiO_3$ substrates were 1 mm thick. Current-voltage and resistance-temperature measurements were done with the configuration shown in (**B**); Hall measurements, with the van der Pauw configuration of (**C**) using either the contact configuration shown in gold or in silver. The charges listed in the lattice sketch represent the unrelaxed charge distribution.

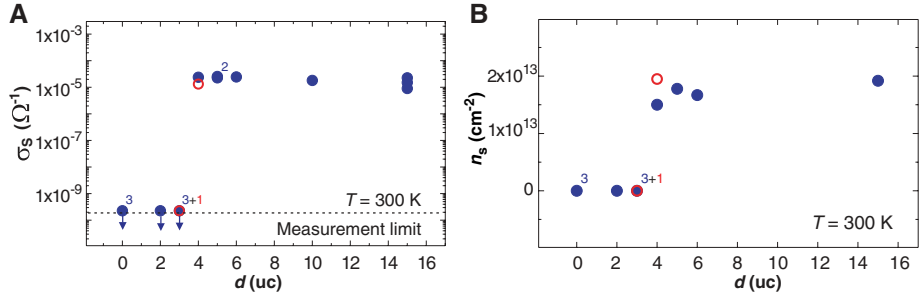

Fig. 2. Influence of $LaAlO_3$ thickness on the electronic properties of the $LaAlO_3$-$SrTiO_3$ interfaces. (**A**) Sheet conductance and (**B**) carrier density of the heterostructures plotted as a function of the number of their $LaAlO_3$ unit cells. The data shown in blue and red are those of samples grown at 770°C and 815°C, respectively. The data were taken at 300 K. The numbers next to the data points indicate the number of samples with values that are indistinguishable in this plot.

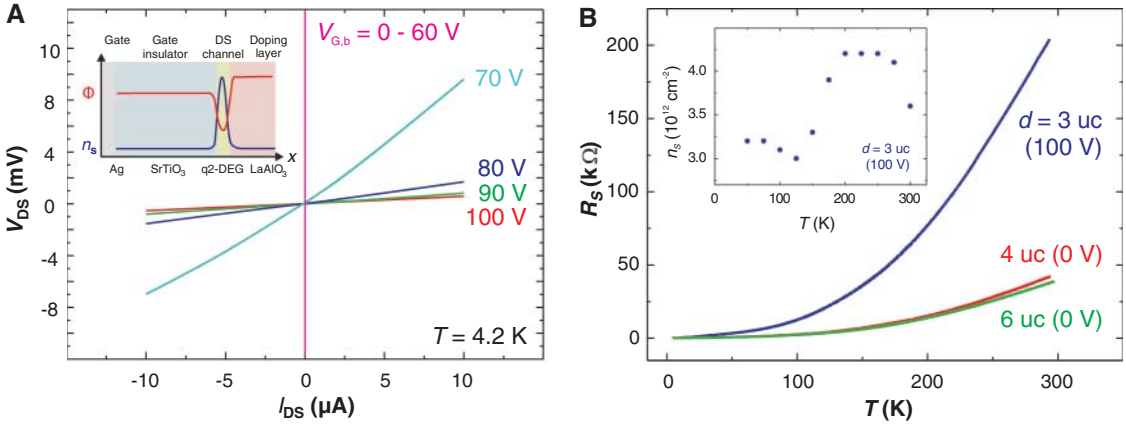

Fig. 3. Transport characteristics of the q2-DEG as a function of applied gate field. (**A**) Voltage-current characteristics of a heterostructure with 3 uc of $LaAlO_3$, measured at 4.2 K with various voltages applied to its back gate. The sample shows a large field-effect response with a conductance change of seven orders of magnitude. The curve taken at $V_{G,b} = 0$ was measured in a two-point configuration, because the resistance was too high to produce a steady voltage between the two voltage contacts of the four-point setup. Several curves display a curvature and an asymmetry, as we observed frequently for high-resistance samples grown on $SrTiO_3$ (*26*). It is attributed to non-ideal and non-identical contacts and to the non-ideal four-point configuration. (Inset) Illustration of the device configuration. Controlled by the spatial dependence $\Phi(x)$ of the electron potential, the q2-DEG is generated at the $SrTiO_3$-$LaAlO_3$ interface, forming the DS channel. (**B**) Sheet resistance measured as a function of temperature for two samples with $d \geq d_c$ at $V_G = 0$ and for one sample with $d = 3$ uc $< d_c$, in which the q2-DEG was induced by $V_{G,b} = 100$ V. The DS current was 1 μA. (Inset) The carrier density of the latter sample (Hall measurements).

painted onto the $LaAlO_3$ (Fig. 1). Also for the gate contacts on 3-uc-thick $LaAlO_3$ layers, the gate resistances were very large (>2 Megohm cm^{-2}), suggesting pinhole-poor (or even pinhole-free) $LaAlO_3$ layers. Independent of which gate electrode was used, pronounced field effects were observed, as anticipated from the weak electrostatic screening of the ultrathin q2-DEG. As illustrated (Fig. 3A), by applying a positive gate voltage, we induced electron gases with sheet conductances as high as $\sigma_s = 5 \times 10^{-3}$ ohm^{-1} (4.2 K) at the interfaces of the 3-uc samples (5×10^{-6} ohm^{-1} at 300 K). The gate field generated metal-insulator transitions with conductance changes exceeding seven orders of magnitude. Driven by the gate voltage and not by thermal activation, this metal-insulator transition is a quantum-phase transition. The sign of the field effect is in accordance with the formation of *n*-doped electron systems.

In samples with $d = 2$ uc, the insulating phase could be barely switched into the conducting one, which shows that the $LaAlO_3$ layers with the subcritical thickness $d = 3$ uc still support the formation of the q2-DEG induced by the electric field. Also in samples with $d \geq 4$ uc, which are already conducting at $V_G = 0$, the conductances were modulated by V_G. However, in these samples a metal-insulator transition could not be induced. According to Hall measurements, the carrier densities of the field-induced q2-DEGs are $\approx 3 \times 10^{12}$ to 4×10^{12} cm^{-2} (Fig. 3); the conductances, mobilities, and $R_S(T)$ dependencies of the field-induced q2-DEGs are reminiscent of the properties of the electron gases that are present in samples with $d \geq d_c$.

The carriers in the DS channels have a high mobility at low *T*. Although not incorporating a spacer layer, these field effect devices are an analog to HEMTs built from conventional semiconductors, because the channel carriers are doped from the $LaAlO_3$ layers, which are spatially separated from the DS channels (Fig. 3A, inset). These

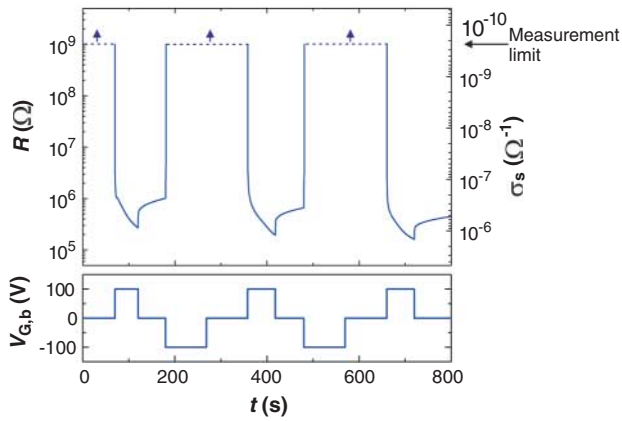

Fig. 4. Memory behavior of the q2-DEG. (**A**) Sheet resistance measured at 300 K and (**B**) applied backgate voltage, both plotted as a function of time for a sample with $d = 3$ uc. By applying the gate voltage pulses, we could reversibly switch the sheet conductance between $\sim 1 \times 10^{-6}$ ohm^{-1} and an unmeasurable value $< 2 \times 10^{-10}$ ohm^{-1}. The data were measured in four-point configurations.

heterostructures apply the concept of modulation doping commonly used in semiconducting heterostructures to oxides (*15*). Yet, there are differences between both systems: On the one hand, the mobilities in the semiconducting interfaces are three orders of magnitude larger than those in the current oxide interfaces, and the carrier densities of the q2-DEG in the oxides exceed those of their semiconductor counterparts by orders of magnitude. Because of the proportionally larger fill factors of the oxide q2-DEGs ($\upsilon = n\Phi_0/B$, where Φ_0 is the magnetic flux quantum and *B* is the applied magnetic flux density), quantum Hall effect–induced resistance oscillations are expected to occur at such oxide interfaces at very large field strengths only. On the other hand, modulation doping of oxides is by principle not restricted to titanates and can be done using many compounds with strongly correlated electron systems. Interactions between the q2-DEG and the correlated electron systems of the bulk may therefore create electronic systems with unique properties.

The field effects shown by the samples are enormous. Field-effect devices that use the $SrTiO_3$ surface as a DS channel have been fabricated with fine characteristics (*16*–*18*), yet the on/off ratios exceed those of these earlier devices by orders of magnitude. There are several reasons: The q2-DEG structures used are close to optimal to achieve large electric-field effects, because the DS channels consist of ultrathin, and therefore weakly screening, electron gases in which a metal-insulator phase transition is induced by the field. In addition, the gate insulator $SrTiO_3$ has a very large electric permittivity (*19*–*21*), which enhances the field response. Furthermore, because there is no conducting DS channel when the sample is insulating, the gate field lines end at the drain and source contacts. Once the gate voltage exceeds a threshold value, the DS channel grows in a bootstrapping mode. This nonlinear process is expected to contribute to the abrupt change of resistance with gate field (Fig. 3).

At 300 K, the electric field–induced q2-DEG was found to display unusual behavior, in particular in samples that over minutes or hours had been subjected to a large $V_{G,b}$ (>70 V). Varying $V_{G,b}$ causes the conductance to react rapidly by a small amount, followed by a larger but very slow change. If the gate is switched, for instance, from $V_{G,b} > 70$ V to $V_{G,b} = 0$ V, the samples with $d < d_c$ retain for hours a high and only slowly diminishing conductance. By application

of a negative $V_{G,b}$, we instantaneously switched off this conductance (Fig. 4). The effect was more pronounced in the samples grown at lower temperature (770°C). Although this memory behavior is reminiscent of ferroelectric field-effect devices (*10*, *22*), the effect is not known for field-effect devices that use dielectric gate insulators.

Within the available V_G window (-2 V < $V_{G,f}$ < 4 V) where V_G also drops along the channel, the memory effect was not found for fields applied via the $LaAlO_3$. Because no mechanism is known that would yield a memory behavior for an isolated q2-DEG, one has to conclude that the $SrTiO_3$ plays a significant role. Indeed, it has been proposed that charge excitations in $SrTiO_3$ can strongly influence the properties of the q2-DEG (*23*). The long, temperature-dependent time constants suggest that creation and motion of defect states, such as oxygen defects, are controlling the dynamics of the effect. We propose that the gate field and also the channel charge give rise to a sheet of positively charged defects or trapping states in the $SrTiO_3$. In this model, the strong electric field of the resulting q2-DEG–defect sheet dipole layer stabilizes the q2-DEG as well as the defect sheet, so that a nominally bistable configuration is obtained. Indeed, being a quantum paraelectric in which the phase transition to the ferroelectric state is suppressed by quantum fluctuations only, already undisturbed bulk $SrTiO_3$ is almost ferroelectric (*24*, *25*).

Operating at 300 K with a large on/off ratio, these field effects are of potential interest for device applications. Although it remains to be clarified whether the device parameters, stability, and integratibility will allow for implementation in practical devices, these heterostructures prove that the coupling of the q2-DEGs to gate fields and to the electronic degrees of freedom of neighboring, complex oxides opens new routes for the design of devices in oxide electronics.

References and Notes

1. H. Koinuma, *Thin Sol. Films* **486**, 2 (2005).
2. A. Ohtomo, H. Y. Hwang, *Nature* **427**, 423 (2004).
3. A. Ohtomo, H. Y. Hwang, *Nature* **441**, 120 (2006).
4. A. S. Kalabukhov *et al.*, http://arxiv.org/abs/cond-mat/papernum=0603501.
5. W. Siemons *et al.*, http://arxiv.org/abs/cond-mat/papernum=0603598.
6. S. M. Sze, Ed., *High-Speed Semiconductor Devices* (Wiley, New York, 1990).
7. A. Ohtomo, D. A. Muller, J. L. Grazul, H. Y. Hwang, *Nature* **419**, 378 (2002).
8. S. Okamoto, A. J. Millis, *Nature* **428**, 630 (2004).
9. J. Mannhart, J. G. Bednorz, K. A. Müller, D. G. Schlom, *Z. Phys. B* **83**, 307 (1991).
10. C. H. Ahn, J.-M. Triscone, J. Mannhart, *Nature* **424**, 1015 (2003).
11. N. Nakagawa, H. Y. Hwang, D. A. Muller, *Nat. Mater.* **5**, 204 (2006).
12. Materials and methods are available as supporting material on *Science* Online.
13. M. Huijben *et al.*, *Nat. Mater.* **5**, 556 (2006).
14. G. Herranz *et al.*, http://arxiv.org/abs/cond-mat/papernum=0606182.
15. H. L. Stormer, *Rev. Mod. Phys.* **71**, 875 (1999).
16. I. Pallecchi *et al.*, *Appl. Phys. Lett.* **78**, 2244 (2001).
17. K. Ueno *et al.*, *Appl. Phys. Lett.* **83**, 1755 (2003).
18. K. S. Takahashi *et al.*, *Appl. Phys. Lett.* **84**, 1722 (2004).
19. O. N. Tufte, P. W. Chapman, *Phys. Rev.* **155**, 796 (1967).
20. H.-M. Christen, J. Mannhart, E. Williams, Ch. Gerber, *Phys. Rev. B* **49**, 12095 (1994).
21. A. Bhattacharya, M. Eblen-Zayas, N. E. Staley, W. H. Huber, A. M. Goldman, *Appl. Phys. Lett.* **85**, 997 (2004).
22. C. H. Ahn *et al.*, *Science* **284**, 1152 (1999).
23. V. Koerting, Q. Yuan, P. J. Hirschfeld, T. Kopp, J. Mannhart, *Phys. Rev. B* **71**, 104510 (2005).
24. K. A. Müller, H. Burkard, *Phys. Rev. B* **19**, 3593 (1979).
25. J. H. Haeni *et al.*, *Nature* **430**, 758 (2004).
26. A. Sawa, C. W. Schneider, J. Mannhart, *Ann. Phys.* (Leipzig) **13**, 595 (2004).

27. We thank H. Y. Hwang, A. Kalabukhov, T. Kopp, G. Koster, G. Sawatzky, D. G. Schlom, and J.-M. Triscone for fruitful discussions and interactions and A. Kalabukhov of Chalmers University for performing the cathodoluminescence studies. S.T. acknowledges fruitful scientific interaction with and hospitality provided by the members of the MESA+ institute at the University of Twente during his stay as a visiting scientist. A.S. thanks the Alexander von Humboldt Foundation for granting a research scholarship. This project was supported by the Bundesministerium für Bildung und Forschung via Verein Deutscher Ingenieure (VDI) (EKM 13N6918), the Deutsche Forschungsgemeinschaft (SFB 484), and the European Science Foundation (THIOX). The financial support of the U.S. Office of Naval Research is gratefully acknowledged.

Supporting Online Material

www.sciencemag.org/cgi/content/full/1131091/DC1
Materials and Methods
Figs. S1 and S2

9 June 2006; accepted 8 August 2006
Published online 24 August 2006;
10.1126/science.1131091
Include this information when citing this paper.

Ultrafast Vibrational Dynamics at Water Interfaces

John A. McGuire* and Y. Ron Shen†

Time-resolved sum-frequency vibrational spectroscopy permits the study of hitherto neglected ultrafast vibrational dynamics of neat water interfaces. Measurements on interfacial bonded OH stretch modes revealed relaxation behavior on sub-picosecond time scales in close resemblance to that of bulk water. Vibrational excitation is followed by spectral diffusion, vibrational relaxation, and thermalization in the hydrogen-bonding network. Dephasing of the excitation occurs in ≤100 femtoseconds. Population relaxation of the dangling OH stretch was found to have a time constant of 1.3 picoseconds, the same as that for excitation transfer between hydrogen-bonded and unbonded OH stretches of water molecules surrounded by acetone.

Water interfaces play an essential role in many physical, chemical, and biological processes. Wetting, corrosion, membrane function, environmental pollution, and soil weathering are just a few familiar examples (*1*, *2*). The properties of both bulk and surfaces of water are governed to a large extent by the network of hydrogen bonds linking the water molecules (*3*). The network is highly dynamic, and recent time-resolved vibrational spectroscopic studies on the sub-picosecond time scale have generated a host of valuable information on hydrogen (H) bonding in bulk water. The focus has been on the OH stretch modes, because they are strongly correlated with H bonding (*3*) and their dynamics over tens to hundreds of femtoseconds reflect directly the dynamics of excitation and relaxation in the H-bonding network (*4*–*6*).

However, hardly any reports on dynamic studies of water interfaces exist in the literature, not because of lack of interest but because of experimental difficulties. Given that water surfaces have a quite different structure than that of the bulk, one might suspect that their vibrational dynamics would be very different as well. Another possibility would be domination of the dynamics in both cases by the H-bonding network, resulting in general similarity of surface and bulk dynamics. Would the reduction of neighbor interactions due to termination of the H-bonding network at the surface make the surface dynamics slower? Alternatively, would the more ordered surface structure lead to faster surface dynamics, as suggested by the observed ultrafast dynamics in isotopically diluted bulk ice compared with bulk water (*7*)?

In recent years, surface-specific sum-frequency vibrational spectroscopy (SFVS) has proven well suited to probing static vibrational spectra of water interfaces. The technique has helped to identify icelike, liquidlike, and dangling OH structures in the terminated H-bonding network of the water interfacial layer (*8*–*12*). In order to probe surface vibrational dynamics of water, time-dependent SFVS is also the technique of choice, although the signal is expected to be much weaker compared with those of the bulk studies. We report here a successful ultrafast dynamics study on neat water interfaces using SFVS. We conducted a surface spectral hole burning experiment in which a femtosecond infrared (IR) pump pulse first created a hole in the spectrum of OH stretches and subsequently time-delayed SFVS probed the evolution of the hole. We observed a recovery time of ~1.3 ps for the dangling OH stretch mode, substantially slower than the OH dynamics in bulk water. In the bonded OH region, however, the observed dy-

Department of Physics, University of California, Berkeley, CA 94720, USA. Materials Sciences Division, Lawrence Berkeley National Laboratory, Berkeley, CA 94720, USA.

*Present address: Chemistry Division, C-PCS, MS-J567, Los Alamos National Laboratory, Los Alamos, NM 87545, USA. †To whom correspondence should be addressed. E-mail: yrshen@calmail.berkeley.edu

Tunable Quasi-Two-Dimensional Electron Gases in Oxide Heterostructures

S. Thiel *et al.*

Science **313**, 1942 (2006);
DOI: 10.1126/science.1131091

Science (print ISSN 0036-8075; online ISSN 1095-9203) is published weekly, except the last week in December, by the American Association for the Advancement of Science, 1200 New York Avenue NW, Washington, DC 20005.